Characterization of metal-biomass interactions in the lanthanum(III) biosorption on Sargassum sp using SEM/EDX, FTIR, and XPS: Preliminary studies

Robson C. Oliveira, Peter Hammer, Eric Guibal, Jean-Marie Taulemesse, Oswaldo Garcia

Characterization of metal–biomass interactions in the lanthanum(III) biosorption on *Sargassum* sp. using SEM/EDX, FTIR, and XPS: Preliminary studies

Robson C. Oliveira [a,*], Peter Hammer [b], Eric Guibal [c], Jean-Marie Taulemesse [c], Oswaldo Garcia Jr. [a]

[a] *Departamento de Bioquímica e Tecnologia Química, Instituto de Química, UNESP – Universidade Estadual Paulista, Rua Prof. Francisco Degni, s/n, CP 14800-900 Araraquara, Brazil*
[b] *Departamento de Físico-Química, Instituto de Química, UNESP – Universidade Estadual Paulista, Rua Prof. Francisco Degni, s/n, CP 14800-900 Araraquara, Brazil*
[c] *Centre des Matériaux des Mines d'Alès, C2MA/MPA/BCI, Ecole des mines d'Alès (EMA), 6, avenue de Clavières, F-30319 Alès cedex, Alès, France*

HIGHLIGHTS

- Metal–biomass interactions in the La(III) biosorption on *Sargassum* were studied.
- FTIR revealed the bidentate complexation of La(III) by alginate carboxylate groups.
- O 1s presented a new phase after metal biosorption.
- La $3d_{5/2}$ confirmed the cooperative action of the biopolymers in the biosorption.
- Si 2p spectra showed that the diatoms did not contribute to the biosorption.

GRAPHICAL ABSTRACT

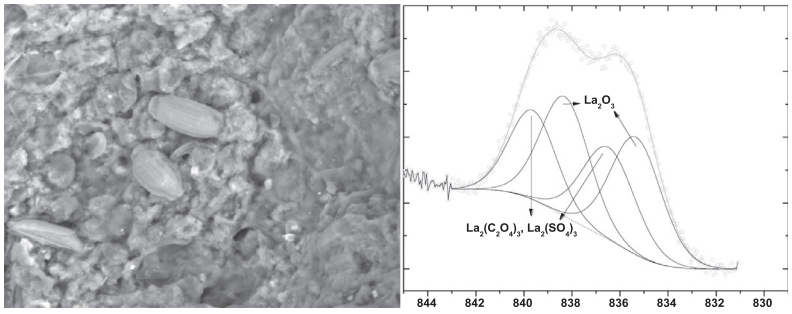

ABSTRACT

This work investigates the mechanisms involved in the biosorption of lanthanum (La(III)) on *Sargassum* sp. biomass using scanning electron microscopy (SEM), SEM coupled to energy dispersive X-ray spectroscopy (SEM/EDX), Fourier transform infrared spectroscopy (FTIR), and X-ray photoelectron spectroscopy (XPS). The biosorbent is characterized by a large heterogeneity of chemical groups constituting different biomass biopolymers and sea compounds. SEM revealed the colonization of *Sargassum* sp. surface by diatoms. SEM/EDX and XPS showed the presence of different chemical groups related to macroalgae, diatoms, and elements of marine environment. FTIR revealed the bidentate complexation of La(III) by alginate carboxylate groups. XPS confirmed that La(III) biosorption occurs via oxygenated compounds: O 1s spectra presented a new phase after metal biosorption; La $3d_{5/2}$ spectra confirmed the cooperative action of the *Sargassum* sp. biopolymers in the biosorption; and Si 2p spectra confirmed that the diatoms did not contribute to the biosorption, at least under selected experimental conditions.

Keywords:
Biosorption
Lanthanum
Sargassum sp.
SEM/EDX
FTIR
XPS

1. Introduction

The need for more effective and economical methods for the removal of heavy metals from aqueous systems has resulted in the development of emerging technologies for metal concentration and separation [1,2]. Conventional physicochemical methods (such as chemical precipitation, electrochemical separation, reverse osmosis, ion-exchange resins, and adsorption resins) for metal removal from wastewaters involve high costs or they are inefficient at low metal concentration or they can generate undesirable secondary residues [3–6]. The biosorption process has been recognized historically as an alternative for concentrating heavy metals from wastewaters of anthropogenic activities [6–16].

* Corresponding author. Tel.: +55 61 35 43 97 60/16 33 01 95 00; fax: +55 16 33 22 23 08.
E-mail addresses: rcebinho@iq.unesp.br (R.C. Oliveira), peter@iq.unesp.br (P. Hammer), Eric.Guibal@mines-ales.fr (E. Guibal).

Biosorption is based on the removal of metal ions from aqueous solution using interactions between metal ions and determined active sites on cellular envelope of biomass (including carboxylate, amino, sulfate, etc.) [9,16–18]. The metal binding occurs as a passive mechanism based on the chemical properties of the cellular envelope: a biological activity is not needed [7,9,18,19]. Both live and dead cells can interact with metal ion species, but dead biomass is generally preferred since (a) the toxicity effects of metals (in high concentrations) do not limit sorption efficiency, and (b) it is not necessary to supply nutrients [2,14,19].

The mechanisms involved in metal accumulation on biosorption sites are numerous and their interpretation is made difficult by the complexity of the biological systems (presence of various reactive groups, interactions between the compounds, etc.) [9,17,20]. Usually these interactions are related to electrostatic interaction, surface complexation, ion-exchange, and precipitation, which can occur individually or in combination [6,8]. The uptake of metal ions starts with the ion diffusion to surface of the biosorbents. Once the ion diffused to cellular surface, it may bind to sites that show some affinity for metal species [7].

The main incentives for biosorption development are: low-cost of biosorbents, high efficiency for metal removal at low concentrations, potential biosorbent regeneration, high velocity of biosorption and desorption, and limited generation of secondary residues [21–23]. A great diversity of biosorbents have been investigated for metal biosorption including fungal biomass [3,13,15–18,24–26], bacteria [3,6,7,13,17,18,24,25,27], algae [8,11–14,18,20,22,25,28–38], biopolymers [5,10,13,25,39–42], and agroindustrial and domestic subproducts [13,25,43,44].

Besides biosorption purposes in the environmental field [1–3,5–11,13–17,19,21–23,26,28,29,35–37,39–44], there is in the literature a crescent interest to apply the biosorption process for the concentration, recovery, and separation of metals of high aggregated value and/or high demand, such as the rare earth (RE) metals [12,13,18,20,24,25,27,30–34,37,38]. RE metals are essential for the manufacturing of a great number of products as a consequence of their peculiar spectroscopic and magnetic properties (e.g. microelectronics, lasers, superconductors, catalysts, etc.) [45–47]. Despite the broad abundance of the RE group in the nature, these metals present high market values. This can be explained by the expensive and complex processes that are needed for separation and purification of RE mixtures. These processes require repeated steps of fractionating by solvent extraction and/or ion-exchange [18,20]. Considering that only few countries and companies detain the complete industrial process of separation of these metals, the biosorption is a potential low-cost alternative for the separation of RE from aqueous systems [18].

Sargassum sp. is found in abundance in several ocean coasts such as in Brazil, Cuba, Australia, USA, and Asian Southeast [20]. Despite the preference for hot waters, this genus is widely spread in temperate to tropical waters because the floatation capabilities conferred by its many air bladders. Other features contributing to rapid spread include: fast growth rate, fertility in the first year, and monoecious reproduction (i.e. both sperm and eggs on the same gametophyte) [48]. A large number of biosorption studies apply to this seaweed because of its broad availability in nature and its well-established commercial exploitation [2,8,12–14,20–23,29–38].

Previous studies showed the potential of *Sargassum* sp. to recover several lanthanide ions (La(III), Pr(III), Nd(III), Sm(III), Eu(III), and Gd(III)) from aqueous solutions in batch systems: the biosorption performance obeys a pseudo-second order kinetics, and sorption equilibrium (sorption isotherms) can be described by the Langmuir adsorption model [12,33]. Furthermore the biosorption (and desorption with HCl 0.10 mol L^{-1}) of La(III) and Nd(III) from binary solutions in fixed-bed columns using *Sargassum* sp. displayed a possible partition between the RE, which is the fundamental condition for separation performance [34].

This work evaluates the mechanisms involved in the biosorption of lanthanum(III) on *Sargassum* sp. biomass using scanning electron microscopy/energy dispersive X-ray spectroscopy (SEM/EDX), Fourier transform infrared spectroscopy (FTIR), and X-ray photoelectron spectroscopy (XPS). The understanding of these mechanisms is required for a better comprehension of biosorption process and its scale-up [13].

2. Theoretical background

2.1. Cell wall biopolymers of Sargassum sp.

Sargassum sp. belongs to *Phaeophyta* group (brown seaweed), whose cellular walls are constituted of a fibrillar skeleton and an amorphous matrix (Fig. A.1, Appendix A). The amorphous matrix is linked to the fibrillar skeleton via hydrogen bonds [49]. The most common fibrillar skeleton is cellulose (2–10% of dry mass) (Fig. A.2, Appendix A) [50].

The amorphous matrix is mainly composed of alginic acid (about 40% of dry mass) or alginate (deprotonated form) (Fig. A.3, Appendix A) besides small amounts of fucoidan (5–20% of dry mass) (Fig. A.4, Appendix A). Fucoidan contains 1-fucose-4-sulfate monomers as major component with sulfate ester ramifications (Fig. A.4, Appendix A) [51]. Despite alginate and fucoidan are also present in fibrillar skeleton, cellulose remains as the main structural component [49,50].

The metal uptake is directly associated to the presence of the alginate carboxylic groups (70% of sites from acid–base titration). The second acidic group is the fucoidan sulfate ester, which may also contribute to biosorption [49]. Alginate is a polysaccharide family containing residues of β-D-mannuronate (M) and α-L-guluronate (G) linked through β(1 → 4) bonds. The residues are arranged in non-regular manner (amorphous) in discrete blocks ordered on chain as $(—M—)_n$, $(—G—)_n$, and $(—MG—)_n$ (Fig. A.3, Appendix A) in four possible types of glycosidic bonds: diequatorial (MM), diaxial (GG), equatorial-axial (MG), and axial-equatorial (GM) (Fig. A.3, Appendix A) [49,50,52].

The biotechnological applications of alginate are based on the biological effects of the polymer itself or on its soft sol/gel transition in the presence of divalent metals (mainly Ca^{2+}) that make the biopolymer an interesting immobilization matrix [49,50,52]. This occurs through metal chelation by dimerized polyguluronic sections $(—G—)_n$, which present high specificity for divalent metals because the zigzag structure readily accommodates metal ions (Figs. A.3 and A.5, Appendix A): the conformation provides a multidentate environment for the coordination (from electrons of the oxygen atoms present in the G ring) [49,50,52,53].

2.2. Diatoms and frustules

Diatoms are the most numerous organisms of the phytoplankton. The frustule (i.e. hard and porous cell wall) of these unicellular algae is composed almost purely of biosilica (essentially SiO_2). Biosilica is metabolically synthesized by the absorption of orthosilicic acid ($Si(OH)_4$) from aqueous media on an organic matrix composed by polysaccharides, proteins, and glycoproteins: the acid molecules are condensed in silica chains into proteic regions (rich in serine and threonine) [54,55].

2.3. Rare earth metals and biosorption

The chemical properties of lanthanides are very similar as consequence of their very close electronic configurations that can be

resumed as [Xe] $4f^n$ $5s^2$ $5p^6$ $5d^{0-1}$ $6s^2$. All neutral atoms have in common a $6s^2$ configuration and a variable occupation of the 4f sublevel (except for lanthanum that has no f electrons in its ground state). However this effect disappears in trivalent ions (more stable thermodynamically in aqueous solution) and a regular increase on $4f^n$ (n = 1–14) configuration is observed [46].

The small chemical differences among lanthanides are used for metal separation by fractionating methods. They are associated to lanthanide contraction of atomic and ionic radius along lanthanide series due to the electrostatic effects in relation with the increase of shielded nuclear charge through partial supply of electron in the 4f sublevel [45,46].

Lanthanide chemical speciation in solution presents a similar behavior for all metals from distinct pH ranges, e.g. lanthanum at pH < 6.0 prevails as La^{3+}; around 6.0 < pH < 9.0 there is variable proportions of $La(OH)^{2+}$ and $La(OH)_2^+$ (solubilized and/or suspended); and $La(OH)_3$ begins to precipitate above pH ~8.5 (Fig. A.6, Appendix A) [56].

RE trivalent ions tend to readily react with oxygen, sulfur, and phosphorus atoms. Thereby it is important to establish the affinity differences among selected elements to propose a process for lanthanide separation and purification through biosorption [31,57].

Usually the RE trivalent ions are coordinated by 8 or 9 waters molecules. In the presence of atoms that are electron donors, these RE aquo complexes form inner sphere complexes [57]. FTIR analyses performed in lanthanum glucuronate complexes displayed the following mechanism: the hydrated metal is coordinated with two oxygen atoms of the carboxylate moieties (bidentate complexes), besides to receive the contribution of electrons from the other oxygen atoms in the glycosidic ring; finally the metal coordination results on partial or total loss of solvated water (Fig. A.7, Appendix A) [58].

3. Materials and methods

3.1. Biomass pre-treatment and sampling for characterization

Sargassum sp. biomass (Rio Grande do Norte, Brazil) was grounded in a blender and the particles with diameter between 0.50 and 2.80 mm were selected. The biomass was subjected to the following washings steps (biosorbent dosage of 10.0 g L^{-1}) with a contact time of 1 h for each step: (a) demineralized water (three times); (b) 0.02 mol L^{-1} HCl (two times); and (c) demineralized water until reaching a pH close to 3.0. Finally, the biomass was dried overnight at 50 °C.

For each characterization (SEM/EDX, FTIR, and XPS) a large amount of pre-treated biomass was exhaustively homogenized and arranged in a conic pile. Three portions from the pile were collected at the bottom, middle, and top, and then the residual pile was homogenized again for a new sampling. This procedure was performed at least ten times. In order to guarantee representative samples, the reserved portions were also homogenized. Before the batch experiments, the reserved biomass was divided in equal fractions for the characterization.

3.2. Lanthanum(III) solutions

Stock solution was prepared from La(III) oxide (La_2O_3, Aldrich 99.9%), which was burned off at 900 °C for 3 h. The oxide was dissolved in small amounts of concentrated HCl under heating before being diluted with demineralized water to reach 5.0 g L^{-1}. The La(III) concentration was standardized by triplicate analysis using the complexometric titration with EDTA in buffer solution of acetate/acetic acid (pH 6.0 ± 0.2) using xylenol orange as indicator.

For biosorption experiments, the solutions were prepared from dilutions of stock solution and pH adjustment to 5.0 ± 0.1 with diluted HCl or NaOH. The metal concentrations in both initial and withdrawn samples were determined in triplicate also by complexometric titration with EDTA for each replicate used in batch biosorption. The selected initial concentrations were 50, 100, and 500 mg L^{-1}, i.e. 0.36, 0.72, and 3.60 mmol L^{-1}, respectively.

3.3. Batch experiments

Biosorption experiments in batch systems were carried out in flasks containing 0.100 ± 0.020 g of pre-treated biomass and 50 mL of La(III) solution (in triplicate) into an orbital shaker with a temperature-controlled environment (G-25 CONTROLLED ENVIRONMENT INCUBATOR – New Brunswick Scientific Co. Inc.) at 150 rpm and 30 °C. Under these experimental conditions, batch blanks with only demineralized water at pH 5.0 ± 0.1 (i.e. without metal, and in triplicate) were performed in order to simulate the pre-treated biomass before the biosorption. After the batch experiments, the biomass samples contained in the flasks for each replicate were grouped for its respective characterization.

The mass balance equation (Eq. (1)) was used to calculate the metal uptake (q, mmol g^{-1}):

$$q = \frac{(C_0 - C_F)}{M} V \quad (1)$$

where V (L) is the volume of metal solution; C_0 and C_F (mmol L^{-1}) are the initial and final concentrations of the metal, respectively; and M (g) is the dry mass of biosorbent.

3.4. SEM/EDX

SEM/EDX analysis were performed on an environmental SEM (FEI Quanta 200 FEG) equipped with X-ray microanalyzer (OXFORD INCA ENERGY 350). The analytical conditions varied as follows: backscattered electrons mode (BSE), magnification of 1096–14,889 times, electron beam voltage of 15 kV, work distance of 10.0–10.4 mm, spot size of 4.0–4.8 nm, pressure of 0.90 Torr, and temperature of 20 °C. The biomass samples were examined before and after La(III) biosorption (using a 3.60 mmol L^{-1} La(III) solution). Under selected experimental conditions the biosorbent reaches the maximum metal uptake (q_{MAX}) close to 0.66 mmol g^{-1} [12].

3.5. FTIR

The samples were pulverized in an agate mortar before being conditioned in KBr pallets and tested in triplicate using NICOLET FTIR IMPACT 400 spectrometer from 4000 to 400 cm^{-1} at a resolution of 4 cm^{-1}. The experiments were carried out from the biomass before and after La(III) biosorption (3.60 mmol L^{-1}). FTIR spectra were plotted ($T = f(wavenumber)$) from the average of the transmittance experimental values. In order to provide the correct assignments (mainly in the shoulders), the method of second-derivative ($d^2T/d(wavenumber)^2 = f(wavenumber)$) was used: the local maxima correspond to the peak position.

The assignments were compared with general literature [59,60] and studies about: (a) biosorption of heavy metals in some specimens of *Sargassum* [8,11,14]; (b) identification of alginate and other biopolymers [61–64]; (c) complexation of heavy metals and RE with mono and disaccharides [58,65–68]; (d) alginate-poly-L-lysine [69,70]; (e) diatoms [54,71]; and (f) carboxylate coordination [72].

The interactions between the carboxylate groups and the La(III) ions were evaluated from the Δ (cm^{-1}) parameter, which is given by Eq. (2) [72].

$$\Delta = \nu_s(COO^-) - \nu_{as}(COO^-) \quad (2)$$

where ν_s (COO^-) and ν_{as} (COO^-) (cm^{-1}) are the wavenumber referred to the carboxylate symmetric and antisymmetric stretching vibrations, respectively.

3.6. XPS

The XPS analysis was performed into the modular system of the SPECS (Berlin) using a UNI-SPECS UHV spectrometer. The Mg Kα line ($h\nu$ = 1253.6 eV) and the analyzer pass energy of 10 eV were used. Charge shift corrections were made by setting the C 1s peak of saturated hydrocarbons to 285.0 eV. After the subtraction of the inelastic background from the Shirley methodology, the composition (in atomic percentage, at.%) was determined from the ratio of the relative peak areas corrected by the sensitivity factors of the corresponding elements. The chemical speciation of the elements were obtained from the high resolution spectra of the core-level for C 1s, O 1s, N1s, S 2p, Si 2p, La 3d, La 4d, Ca 2p, and Al 2p. The experimental data were fitted by Voigt functions (GL(30)). The full-width at half-maximum was adjusted according to each component between 1.4 and 2.6 eV, and the accuracy of the peak position was ±0.10 eV.

The biomass samples were analyzed before and after La(III) biosorption (using concentrations set to 0.36, 0.72, and 3.60 mmol L^{-1}). The assignments were inferred in accordance with references related to: (a) adsorption of heavy metals in several biomasses, biopolymers, and synthetic polymers [8,10,14,15,40,42,64,69,73–75]; (b) lanthanide inorganic compounds (oxides, sulfates, silicates, and oxalates) [76–78]; and (c) XPS electronic database [79].

4. Results and discussion

4.1. SEM/EDX

Fig. 1 presents an electron micrograph example of the biosorbent after La(III) binding (q = 0.656 ± 0.003 mmol g^{-1}), where several sites on the biomass are analyzed and their respective X-ray spectra are shown (other micrographs in Figs. B.1–B.3, Appendix B).

The surface of *Sargassum* sp. is colonized by distinct diatoms with a non-homogeneous distribution (Fig. 1). The diatom colonization can be promoted by the production of exopolymeric substances (EPS) that help the diatom adhesion on biomass surface [80]. However, EPS did not appear systematically and in some cases the diatoms seem to be fixed directly to the macroalga surface or interweaved in their fibers (Fig. 1, and Figs. B.1–B.3, Appendix B).

Table 1 summarizes the chemical groups that could appear on the cellular envelopes of *Sargassum* sp. and diatoms. The elements of the expected chemical groups, contained on Table 1, were present in practically every tested micrograph segment (Fig. 1, and Figs. B.1–B.3, Appendix B); the only exception was nitrogen that appeared once (spectrum (3) in Fig. B.1, Appendix B), due to its low relative quantity and low analytical sensitivity.

Besides the compounds cited on Table 1, other compounds can be precipitated or adsorbed on biosorbent surface such as salts, oxides, hydroxides, and oxohydroxides originally dissolved or suspended in the sea water: e.g. compounds containing aluminum, calcium, chlorine, iron, potassium, magnesium, phosphorus, sulfur, silicon, and titanium (Table B.1, Appendix B). The deposition/formation of the compounds cited above on the biosorbent is based on the biomineralization processes that can be mainly biologically-controlled or biologically-induced [81].

As expected, EDX spectra confirm that silicon content is higher in the presence of diatoms. Nevertheless silicon, calcium, and aluminum assignments are present in each of these spectra (Fig. 1, and Figs. B.1–B.3, Appendix B). In addition on some spectra it was possible to observe the presence of iron (spectra (1–3) in Fig. 1; and Fig. B.2, and on spectrum (1) in Fig. B.3, Appendix B). Moreover the peaks related to potassium, chlorine, and magnesium before metal biosorption (Figs. B.1 and B.2, Appendix B) disappeared after La(III) biosorption (Fig. 1, and Fig. B.3, Appendix B). These elements were probably ion-exchanged with La(III). As will be shown below, XPS data give a support for this suggestion.

After metal biosorption (Fig. 1, and Fig. B.3, Appendix B), lanthanum assignments are included in practically every scanned region, which suggests that the metal sorption occurs in both seaweed and diatoms. The only exception was the spectrum (1) on Fig. 1 that did not present lanthanum, but it displayed a titanium peak (probably a laboratory contamination).

4.2. FTIR

Fig. 2 shows the transmission spectra for *Sargassum* sp. before and after La(III) biosorption (q = 0.664 ± 0.007 mmol g^{-1}). Fig. 2a and Table 2 report the assignment of principal absorption bands, which are consistent with compounds found in the biomass (Table 1): hydrocarbons (CC, CH), alcohols (COH), ethers (COC), amines/amides (CN, NH), sulfonate and sulfate (SO_3^- and SO_4^{-2}, related to sulfate ester, $COSO_3^-$), carboxylic acid/carboxylate (COOH/COO^-), and silica/silanol (SiOSi/SiOH). However the assignment of several bands is made difficult due to the superimposition of peaks.

In general, Fig. 2a and Table 2 did not show systematic shifts of the bands after La(III) biosorption, but punctual and discrete shifts of certain bands that allow infer the possible groups involved on metal adsorption. The region between 3700 and 3000 cm^{-1} (Table 2) corresponds to hydroxyl stretches in several compounds, and amines and amides in amino acids. This band is broad (Fig. 2a) because of the high number and large density of hydrogen bonds, mainly hydroxyl radicals in the polysaccharide pyranose rings. Table 2 reports also hydrocarbon stretches between 2930 and 2860 cm^{-1}.

The carbonyl stretching of carboxylic acids appears close to 1730 cm^{-1} (Table 2). This band indicates that a fraction of the carboxylic sites is not deprotonated even in the presence of La(III); while the other fraction is deprotonated as shown by the antisymmetric and symmetric stretches of carboxylate groups at 1640 cm^{-1} and 1430 cm^{-1} (Table 2), respectively. The first wavenumber also corresponds to the vibrations of primary amides in amino acids, but the band intensity is mainly attributed to alginate carboxylate. On the other hand, the presence of amino acids is confirmed by the peak at 1540 cm^{-1} (Table 2), which is associated to peptide bonds in proteins and glycoproteins (secondary amides).

Fig. 2b shows the three "well-defined" bands before and after La(III) biosorption; after metal binding, the amide band tends to superimpose with carboxylate bands, leading to the broadening of this band. This phenomenon is probably due to the interaction of carboxylate anions with La(III). Indeed, similar behavior was verified by Oliveira (2011) for the biosorption of neodymium(III), europium(III), and gadolinium(III) on *Sargassum* sp. at 3.60 mmol L^{-1} (Fig. C.1, Appendix C) [82].

Starting from the assumption that the alginate carboxylate groups carry out the largest share of biosorption, the Δ parameter (Eq. (2)) was calculated to evaluate the coordination environment of these groups with La(III). Table 2 reports the wavenumbers of carboxylate stretches used for the calculation of Δ parameter, whose values found were 213 and 214 cm^{-1} for *Sargassum* sp. before and after La(III) biosorption, respectively (close to other RE studied by Oliveira [82], Table C.1, Appendix C). These results are consistent with those obtained in other studies for the biosorption

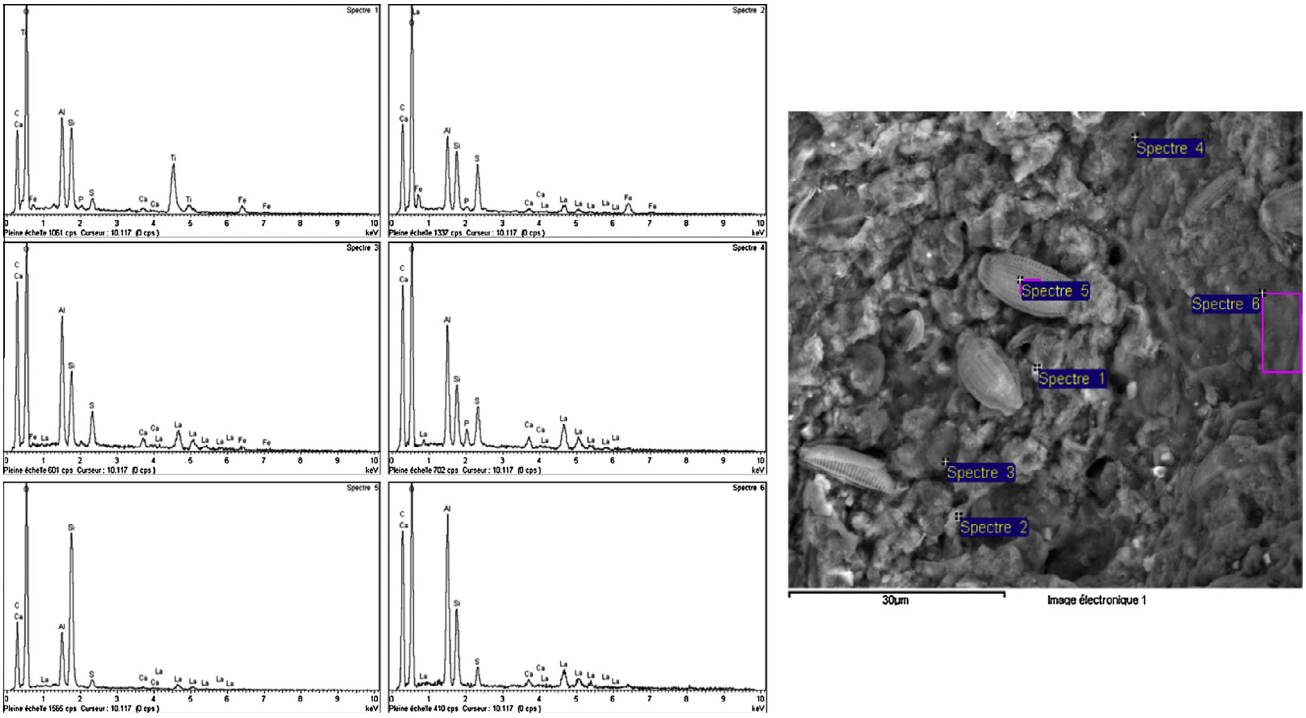

Fig. 1. Scanning electron micrograph of the biomass after lanthanum(III) biosorption at 3.60 mmol L^{-1} and selected X-ray spectra: (1), (2), (3), (4), and (6) for *Sargassum* sp., and (5) for diatom.

Table 1
Probable chemical groups, acid groups, their pK_as, and associated compounds on cellular envelopes of *Sargassum* sp. and diatoms.

Chemical groups	Acid group	pK_a	Associated compounds
CH, CC	–	–	Polysaccharides, proteins, glycoproteins
COH, COC, OCO	COH	10–13	Polysaccharides and glycoproteins
COOH, COO^-	COOH	2–5	Alginate, proteins, and glycoproteins
$COSO_3H$, $COSO_3^-$	$COSO_3H$	<2	Fucoidan
CNH, CNH_2, CNH_3^+	CNH_3^+	9.5–11	Proteins and glycoproteins
(CO)NH, $(CO)NH_2$, $(CO)NH_3^+$	$C(O)NH_3^+$	9–11	Proteins and glycoproteins
SiOSi, OSiO, SiOH	SiOH	7–8	Biosilica
$COPO_2H$, $COPO_2^-$	$COPO_2H$	<3	Phospholipids

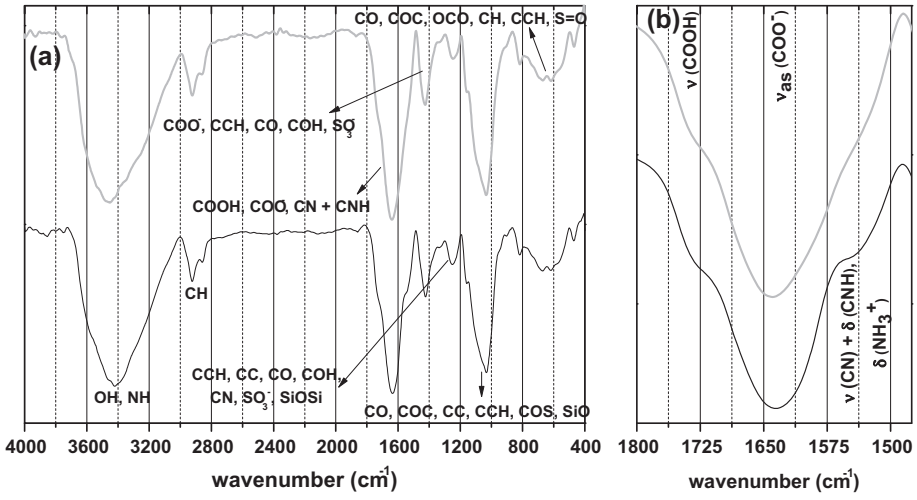

Fig. 2. Infrared spectra for *Sargassum* sp. before (—) and after (——) lanthanum(III) biosorption at 3.60 mmol L^{-1}: (a) total spectra (4000–400 cm^{-1}) and (b) partial spectra (1800–1475 cm^{-1}), and respective assignments.

Table 2
Band assignments of the FTIR spectra for *Sargassum* sp. before (Sarg.) and after (La) lanthanum(III) biosorption at 3.60 mmol L^{-1}. Symbols: s, shoulder; ν, stretching; δ, bending; τ, internal rotation; ω, wagging. The values in bold were used for the calculation of the Δ parameter (Eq. (2)).

Sarg. (cm^{-1})	La (cm^{-1})	Possible assignments
3700–3000		ν (OH): sugars, amino acids e biosilica; ν (NH): amino acids
2924	2922	ν (CH) α-anomeric: sugars; ν (CH) antisymmetric: mainly sugars
2858	2862	ν (CH) β-anomeric: sugars; ν (CH) symmetric: mainly sugars
1728 (s)	1728 (s)	ν (C═O) in COOH: alginate and amino acids
1636	**1639**	ν (CO_2^-) antisymmetric: alginate and proteins; ν (C═O) + ν (CN) + δ (NH) in primary amides: amino acid side chains
1539 (s)	1531 (s)	δ (NH_3^+) antisymmetric: N-terminal amino acids; ν (CN) + δ (CNH) in secondary amides: peptide bond
1423	**1425**	ν (CO_2^-) symmetric: alginate and amino acids
1381 (s)	1375 (s)	ν (CC) + δ (COH) + δ (OCH) + δ (CCH) + δ (CCO) + τ (CCCH): mainly sugars; ν (O═S═O) antisymmetric in sulfonate: fucoidan
1325 (s)	1333 (s)	δ (COH) + δ (OCH) + δ (CCH) + ν (CO) + τ (CCCH) + ω (CH): mainly sugars
1252	1247	ν (CO) in COOH: alginate and amino acids; ν (CNC): amino acids; ν (S═O) in sulfate: fucoidan; δ (CCH) + δ (COH) + δ (OCH): mainly sugars
1159	1157	ν (CO) + ν (CC) + ν (COC) + δ (COH): mainly sugars; ν (CN): amino acids; ν (O═S═O) symmetric in sulfonate: fucoidan; ν (SiOSi) antisymmetric: biosilica
943 (s)	945 (s)	ν (CO) + ν (CC) + ν (CCH) + δ (CO) + δ (CCO) + τ (CCCC) + τ (OCCC): mainly sugars; α (1 → 4) glycosidic bond in alginate
901	903 (s)	ν (CO) + ν (CC) + δ (CC) + δ (CCH) + τ (CCCC) + τ (OCCC): mainly sugars; ν (pyranose ring): sugars; δ (CH) β-anomeric: sugars; ν (COS) symmetric: fucoidan; ν (SiO) in SiOH: biosilica
818	818	δ (CCO) + δ (CCH) + τ (CO): mainly sugars; δ (CH) α-anomeric: sugars; M residues in alginate; δ (COS): fucoidan; ν (SiO) in SiOH: biosilica
781 (s)	779 (s)	ν (COC) + δ (CCO) + δ (CCH) + τ (CO): mainly sugars; ν (pyranose ring): sugars; G residues in alginate
737 (s)	741 (s)	ν (CH) + ν (CC) + δ (CCO) + δ (CCH) + δ (CCC) + δ (OCO) + τ (CO) + τ (OCCC): mainly sugars; ω (NH): proteins
671	669	ν (CH) + ν (CC) + δ (CCO) + τ (CCO) + τ (CCCC) + τ (OCCC): mainly sugars; ν (O═S═O) in sulfate: fucoidan
619	617	δ (CCO) + τ (CCO): mainly sugars; ν (O═S═O) in sulfate: fucoidan
555 (s)	557 (s)	δ (CCO) + τ (CO): mainly sugars; δ (O═S═O) antisymmetric: fucoidan; ν (O═S═O) in sulfate: fucoidan
471	469	δ (CCO) + τ (CO): mainly sugars; τ (CO) β-anomeric: sugars
424 (s)	420 (s)	δ (CCO) + δ (CCH): mainly sugars

of heavy metals in *Sargassum* sp. [8,11,14] and for RE(III) complexation with uronic acids [58]. They are commonly related to the formation of bidentate complexes.

Table 2 displays for both carboxylate bands a small displacement to higher wavenumber after metal biosorption. It has been suggested that symmetrical bridging and chelation (bidentate complexes) shift the CO_2^- bands in the same direction [72] (similarly to other RE studied by Oliveira [82], Table C.1, Appendix C). Thus this behavior can confirm the mechanism of metal coordination.

The heterogeneity of the biomass (even with its "homogenization"), the discrete changes observed in the FTIR spectra, and the equipment resolution could impair the description of a mechanism. Nevertheless the mechanism described in the manuscript was suggest based on the good reproducibility of the results (experimental errors lower than ±1 cm^{-1}), due to the precise assignment of the positions of the carboxylate bands (Table 2 and Table C.1, Appendix C), and similar shape of the curves after the biosorption of La(III) and other RE studied by Oliveira [82] (Fig. C.1, Appendix C).

The band at 1380 cm^{-1} is assigned to antisymmetric stretching in sulfonate from fucoidan (Table 2). Though other assignments may be inferred in this shoulder, this region is usually correlated to fucoidan in *Sargassum* sp. [8,11,14]. Combined vibrations related to bending in hydroxyl groups from alcoholic groups in sugars are observed at 1320 cm^{-1} (Table 2).

The region between 1250 and 1000 cm^{-1} shows assignments mainly attributed to oxygenated groups (C—O bonds) in alcohols, ethers, and carboxylic acids (in sugars): they are not affected by metal binding. The bands between 1000 and 400 cm^{-1} correspond to sugar vibrations.

The diatom contribution appears as siloxane (Si—O—Si, strong band in the range 1130–1000 cm^{-1}) and/or silanol (Si—OH, detected by several bands between 3700 and 3000 cm^{-1} and a strong band in the region of 910–830 cm^{-1}). Nevertheless these assignments are not easy to identify on spectra (Fig. 2) because of their superimposition or convolution with other vibrations.

4.3. XPS

Some preliminary comments are necessary before discussing the XPS data. The pre-treatment with a slightly acidic washing contributes to stabilize the biomass, removes metals and adsorbed compounds from sea, and prevents further leaching of organic compounds. This stabilization contributes to reduce pH variation that may occur during metal sorption [33]. Furthermore, the protonation optimizes the biosorption performance. La(III) biosorption increases the pH from 2.0 to 5.0 [20,82] as a function of the change in the ionic state of the carboxylic groups to carboxylate. This behavior can be explained by the ion-exchange of protons at biomass active sites and metal ions in solution.

The biomass was loaded with La(III) solutions at concentrations of 0.36, 0.72, and 3.60 mmol L^{-1}, corresponding to different levels of saturation of the biomass (0.159 ± 4.8E−04, 0.343 ± 0.004, and 0.652 ± 0.005 mmol g^{-1}: i.e. 25%, 50%, and 100% of q_{MAX}, respectively) [12]. At the end of the pre-treatment of the biosorbent the pH of the solution was close to 3. While the initial pH of La(III) solutions was 5.0 ± 0.1, at equilibrium the pH was shifted to values between 3 and 4. Table 1 reports the speciation of the acid groups before, during, and after metal biosorption. The changes occur according their respective pK_as. Based on the tested pH values (independently of La(III) binding), the speciation of these groups may be: COOH/COO^- at equilibrium, $COSO_3^-$, CNH_3^+, SiOH, COH, $COPO_2^-$ (Table 1).

Table 3 lists the composition of the biomass surface before and after lanthanum(III) biosorption at concentrations of 0.36, 0.72, and 3.60 mmol L^{-1} from the XPS survey spectra (Fig. D.1, Appendix D).

SEM micrographs (Fig. 1, and Figs. B.1–B.3, Appendix B) have shown the heterogeneous distribution of diatoms over the surface.

Table 3
Composition in atomic concentration (C) of elements identified, binding energy (E_B), and percentage of the peak area (% A) of the deconvoluted components in the XPS spectra for *Sargassum* sp. before and after lanthanum(III) biosorption at 0.36, 0.72, and 3.60 mmol L^{-1}.

			Sargassum sp.			La(III) 0.36 mmol L^{-1}			La(III) 0.72 mmol L^{-1}			La(III) 3.60 mmol L^{-1}		
Element[a]	Core-level	Assignment	C (at.%)	E_B (eV)	% A	C (at.%)	E_B (eV)	% A	C (at.%)	E_B (eV)	% A	C (at.%)	E_B (eV)	% A
C	1s	C—C/C—H/C_{ADS}	55.5[b]	285.0	63.0	53.8	285.0	51.7	52.9	285.0	50.7	54.9	285.0	67.6
		C—O		286.6	25.3		286.7	35.7		286.6	35.2		286.7	20.3
		C=O/O—C—O		288.2	9.3		288.3	8.9		288.3	12.9		288.3	10.5
		COO^-		289.4	2.4		289.3	3.7		289.6	1.2		289.6	1.6
O	1s	La—O	33.3	–	–	35.4	529.7	1.6	35.7	529.4	0.7	34.6	529.5	1.5
		O—H/SO_3^-/Al_2O_3		531.4	18.6		531.4	17.8		531.5	25.0		531.3	15.2
		C=O/C—O		532.5	61.3		532.6	55.8		532.6	55.6		532.4	61.8
		Si—O/COO^-		533.4	20.1		533.3	24.8		533.4	18.7		533.4	21.5
N	1s	N—C=O/NH_2	2.2	400.0	96.7	3.6	400.0	96.1	3.7	400.0	95.5	2.1	400.1	95.4
		NH_3^+		402.3	3.3		402.3	3.9		402.1	4.5		402.4	4.6
S	2p	OSO_3^- $2p_{3/2}$	1.5	169.0	73.1	1.1	169.1	67.7	0.9	169.0	69.5	1.4	168.9	63.2
		OSO_3^- $2p_{1/2}$		170.2	26.9		170.2	32.3		170.2	30.5		170.0	36.8
Si	2p	SiO_2	5.0	103.5	100	4.9	104.0	100	5.4	103.8	100	5.2	103.5	100
La	3d	La_2O_3	–	–	–	0.1	835.2	31.5	0.3	835.2	29.5	0.6	835.3	28.7
		$La_2(C_2O_4)_3$/$La_2(SO_4)_3$		–	–		836.6	24.9		836.6	27.0		836.5	23.3
		La_2O_3 shake-down		–	–		838.3	26.6		838.3	24.4		838.3	27.8
		$La_2(C_2O_4)_3$/$La_2(SO_4)_3$ shake-down		–	–		839.5	17.0		839.5	19.1		839.6	20.2
	4d	La $4d_{5/2}$		–	–		107.2	100		107.0	100		106.8	83.1
		La $4d_{3/2}$		–	–		–	–		–	–		109.3	16.9
Ca[c]	2p	Ca $2p_{3/2}$	1.0	347.9	67.6	0.1	–	–	0.1	–	–	–	–	–
		Ca $2p_{1/2}$		351.5	32.4		–	–		–	–		–	–
Al[c]	2p	Al^0 or AlN	1.5	–	–	1.0	–	–	1.0	–	–	1.2	73.2	4.7
		Al_2O_3		–	–		–	–		–	–		74.9	95.3
Total	–	–	100	–	–	100	–	–	100	–	–	100	–	–

[a] The composition of some trace elements (Fe, Mg, P, and Cl) was not represented due to the low signal to noise ratio, close to the detection limit (0.1 at.%).
[b] Experimental error: ± 5%.
[c] Despite these elements are present in pratically all samples, their high-resolution spectra were determined only in some of the evaluated conditions.

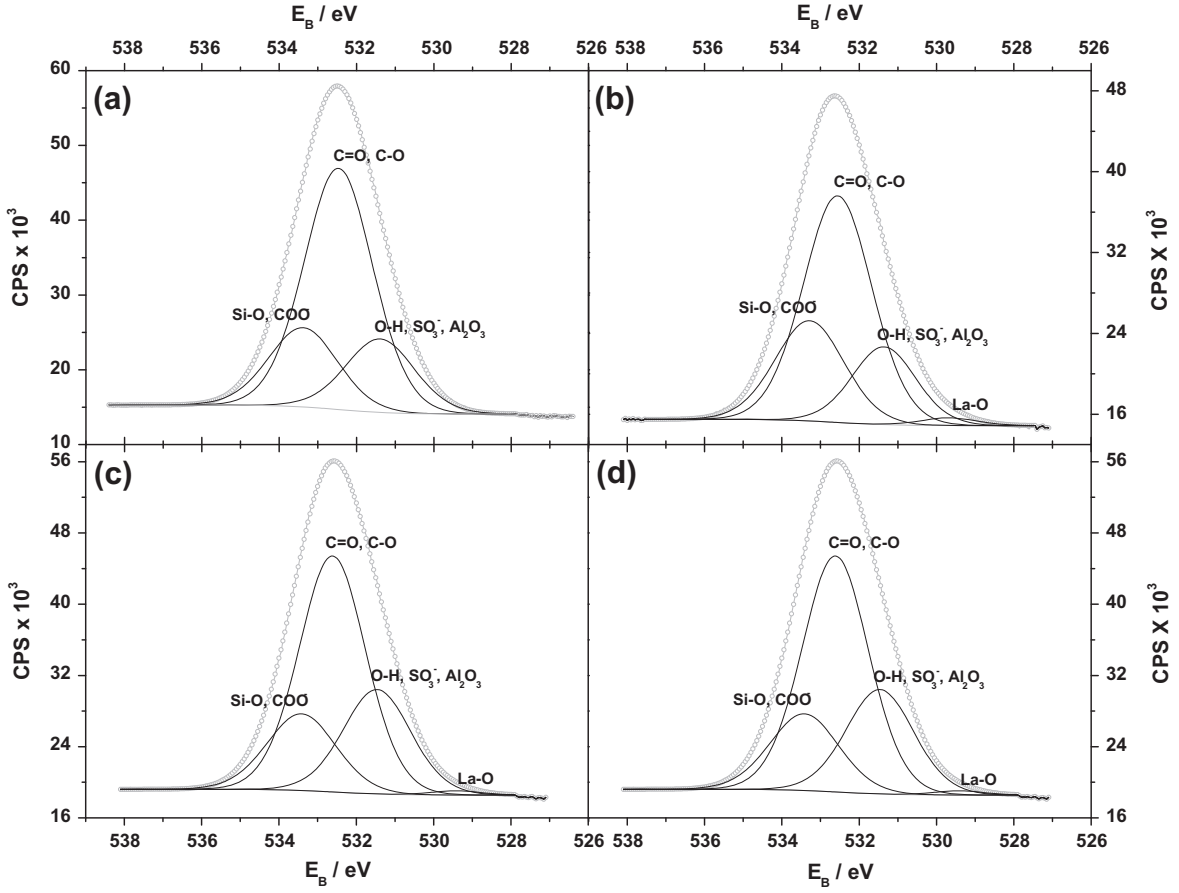

Fig. 3. Fitted high-resolution photoemission spectra of the O 1s core-level for *Sargassum* sp.: (a) before and after lanthanum(III) biosorption at (b) 0.36 mmol L^{-1}, (c) 0.72 mmol L^{-1}, and (d) 3.60 mmol L^{-1}, and respective assignments. Label: (○) recorded signals by the equipment; (——) baseline and Voig-type fitted curve for the elastic peak; and (—) deconvoluted regions from the fitted curve.

On the other hand, EDX and XPS analyses indicate that silicon, carbon, and oxygen are relatively homogeneously distributed, with similar concentrations for all samples (Table 3).

The elements identified by EDX (Fig. 1, and Figs. B.1–B.3, Appendix B) (iron, phosphorus, magnesium, and chlorine) were found at trace levels (i.e. the sum of these elements is less than 1.0 at.%). Calcium is present in much higher proportion before La(III) biosorption. After metal biosorption its atomic percentage decreased for La(III) at 0.36 and 0.72 mmol L^{-1} and then further reduced below the detection limit as the metal concentration reached 3.60 mmol L^{-1} (Table 3). This clearly indicates that the calcium was replaced by La(III) ions. The ion-exchange of magnesium by La(III) is also supported by the XPS data, showing a decreasing concentration, from about 0.5 at.% to a value close to the detection limit (0.2 at.%), after La biosorption. A similar tendency was expected for other trace elements like iron, phosphorous, and chlorine, however their low signal to noise ratio, close to the detection limit (0.1 at.%), prevented to establish a clear correlation. Aluminum was also detected in all samples (Table 3 and Fig. D.1, Appendix D). Finally, the atomic percentages of lanthanum increased for the three biosorption conditions, consistently with the levels of expected metal uptake (q) (Table 3 and Fig. D.1, Appendix D).

Table 3 illustrates the complexity of the chemical composition of the biomass: the biosorbent has a heterogeneous surface composition due to its multicellular organization. It should be noted that XPS is a surface technique that analyzes the first monolayers (<4 nm) of the sample. Considering the entire volume of the biosorbent, obviously a lower contribution of the diatom biosilica and substances deposited on the biosorbent surface from marine environments it is expected. Another important observation is that although the most of the biosorption occurs at the surface, it also might take place in reduced extent throughout the volume of the biosorbent particles due to the porosity of the material.

Therefore, the experimental results allowed an initial semi-quantitative estimate of different chemical groups in the near surface region of the biomass before and after metal sorption.

4.3.1. Spectral C 1s line

Table 3 (and Fig. D.2, Appendix D) shows the assignments of the components obtained from the deconvolution of the C 1s line. The data show no systematical changes of the assigned chemical states for the biomass before and after La(III) biosorption. Assuming that the carbon distribution is relatively homogeneous (Table 3), for the peak at 285 eV, related to hydrocarbons and adsorbed carbon, no significant intensity change is expected. The observed peak area variation (larger than 10%) of this component can be related to the surface heterogeneity of hydrocarbon-containing portions and the presence of a large number of different C—O groups.

4.3.2. Spectral O 1s line

Fig. 3 and Table 3 show the assignments of the deconvoluted components of the O 1s spectra. It can be observed that the quantitative peak area distribution of C—O components is similar to that of the C 1s line. In general, the spectra are quite similar for all samples, formed by components related to the presence of a large number of chemical groups containing oxygen. After La(III) biosorption, however, a new peak emerged as a the low energy tail (529.4–529.7 eV). This binding energy is commonly related to lanthanum oxide (La_2O_3) [77,78]. On La(III)-loaded biosorbent, this peak is probably associated with the interactions of La(III) with oxygen atoms of chemical groups present at the surface of the material.

4.3.3. Spectral N 1s line

Table 3 (and Fig. D.3, Appendix D) displays the fitted N 1s spectra. The area of the main peak decreased slightly with increasing of

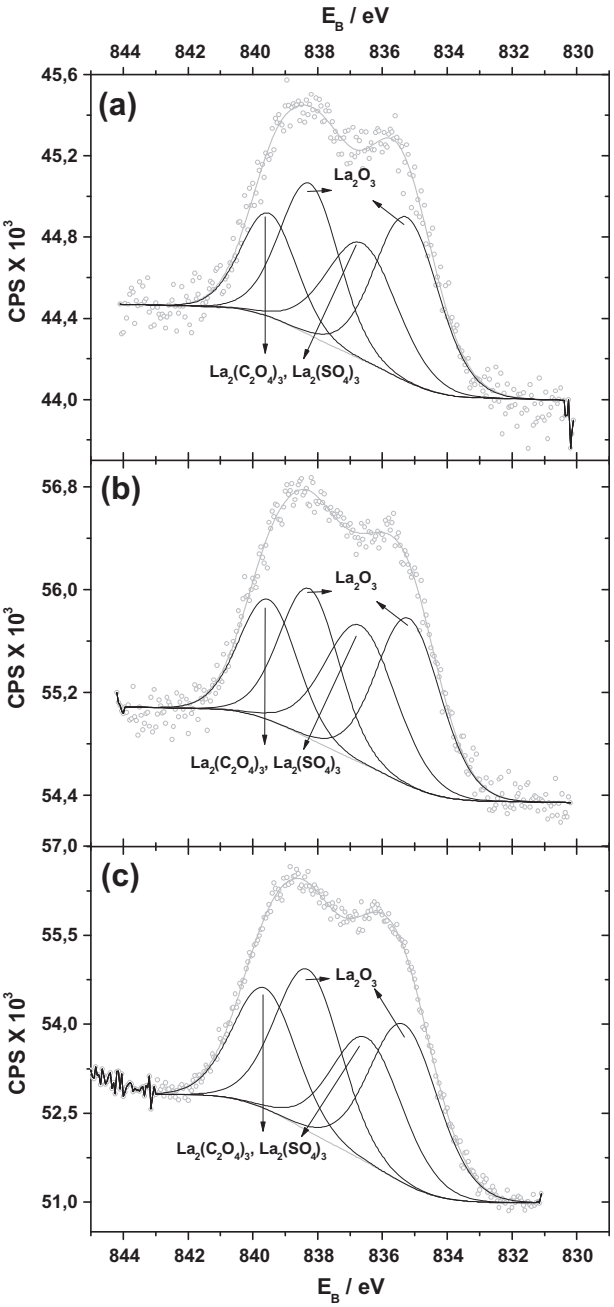

Fig. 4. Fitted high-resolution photoemission spectra of the La $3d_{5/2}$ core-level for *Sargassum* sp.: after lanthanum(III) biosorption at (a) 0.36 mmol L^{-1}, (b) 0.72 mmol L^{-1}, and (c) 3.60 mmol L^{-1}, and respective assignments. Label: (○) recorded signals by the equipment; (——) baseline and Voig-type fitted curve for the elastic peak; and (—) deconvoluted regions from the fitted curve.

La(III) concentration. As the pH decreases during sorption, this may explain the increasing protonation of amine groups is expected, confirmed by the increase of the area of NH_3^+ component (~ 402 eV). The interaction of metal ions with nitrogen (coordination by amine groups) is another possible explanation for small increase of this peak, as it is reported for Cu(II) biosorption in chitosan [10].

4.3.4. Spectral S 2p line

Table 3 (and Fig. D.4, Appendix D) shows the assignments for the S 2p spectra. Sulfur is present in sulfate forms, as deduced from the high chemical shift of about 5 eV (compared to elemental S)

and energy separation (i.e. 1.1–1.2 eV) observed in the S $2p_{3/2}$ and S $2p_{1/2}$ degenerated orbitals [8]. The sulfate is related to fucoidan sulfate ester groups. The fact that after La(III) biosorption these bands are not affected suggests that the amount of La(III) interacting with these groups is not sufficient to be detectable.

4.3.5. Spectral La 3d line

Fig. 4 and Table 3 shows the deconvoluted La $3d_{5/2}$ spectra. The low amount of adsorbed metal (between 0.1 and 0.6 at.%, in Table 3) explains the high noise of the recorded signal (Fig. 4). Moreover there is the occurrence of typical shake-down peaks for the $3d_{5/2}$ orbital in lanthanides oxides: the phenomenon is related to a fraction of lanthanum atoms that decay during photoemission process under loss of a small portion of energy due the valence band excitations (O 2p to La 4f transitions); consequently, a part of the photoelectron intensity occurs as satellite bands at higher binding energies [76,77].

The components at 835.2 eV and 838.3 eV were attributed to lanthanum oxide (La_2O_3), whereas the possible assignment of the peaks at 836.6 eV and 839.5 eV is lanthanum oxalate ($La_2(C_2O_4)_3$, i.e. $La_2(^{-}OOC{-}COO^{-})_3$) or lanthanum sulfate ($La_2(SO_4)_3$) [77]; thereby these doublets (elastic peak plus shake-down peak) must be interpreted as the result of the interaction of La(III) ion with oxygen atoms: (a) the first doublet from alcohol and ether groups (in polysaccharides), and (b) the second doublet from carboxylate (in alginate and amino acids) and sulfate ester groups (in fucoidan). These results corroborate with the appearance of the small band of the O 1s core-level (529.4–529.7 eV) after metal biosorption (Fig. 3 and Table 3). Consequently, these two spectra indicate that La(III) adsorbed to the biomass is essentially bonded via oxygenated groups.

Finally, the spectral components, enumerated in Table 3, did not show any systematic changes with increasing La(III) concentration; however, they revealed that La(III) ions are adsorbed on biosorbent surface through distinct interactions (Fig. 4), which act cooperatively for metal coordination.

4.3.6. Spectral Si 2p and La 4d lines

Fig. 5 and Table 3 display the fitted Si 2p spectra and the superimposed La 4d lines after La(III) biosorption. Silicon is present in the form of silica (SiO_2, at 103.5 eV) in all samples (as biosilica on diatom frustules). As there is no significant change of Si-O binding energy, this indicates that La(III) is probably not interacting with the diatom material. The weak binding ability of diatom frustule for La(III) is probably due to the acidity of the solution (between 3 and 5). This result contrasts with data reported by González-Dávila et al. for copper biosorption at pH 8 using diatoms such as *Thalassiosira weissflogii* and *Phaeodactylum tricornutum* [28].

4.3.7. Spectral Ca 2p and Al 3p lines

Table 3 (and Fig. D.5, Appendix D) shows the fitted spectra of Ca 2p and Al 3p lines. Table 3 shows an initial calcium content of 1.0 at.%, and the following decrease below the detection limit

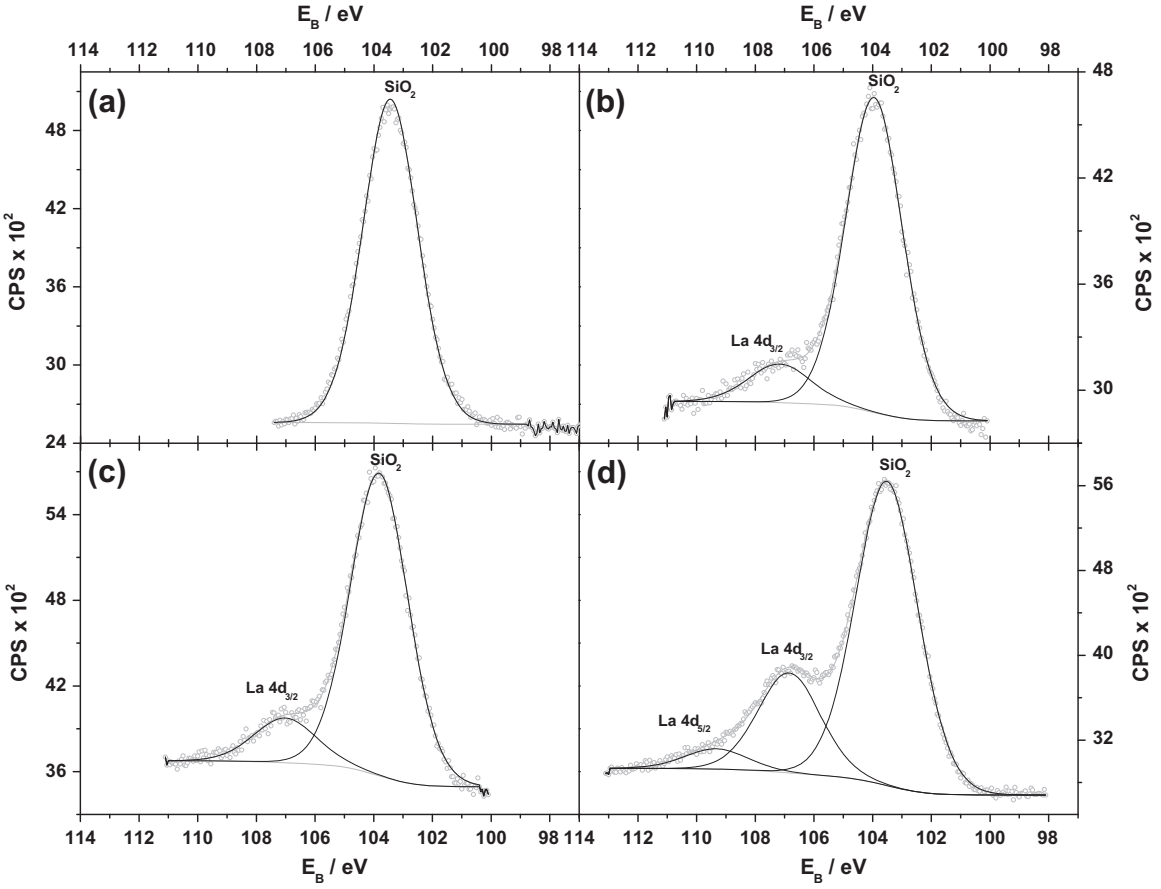

Fig. 5. Fitted high-resolution photoemission spectra of the Si 2p and La 4d core-levels for *Sargassum* sp.: (a) before and after lanthanum(III) biosorption at (b) 0.36 mmol L^{-1}, (c) 0.72 mmol L^{-1}, and (d) 3.60 mmol L^{-1}, and respective assignments. Label: (○) recorded signals by the equipment; (——) baseline and Voig-type fitted curve for the elastic peak; and (—) deconvoluted regions from the fitted curve.

(0.1 at.%) after La(III) biosorption. As already stated, initially this element is bonded to oxygenated compounds, consistently with the peak position of the Ca $2p_{3/2}$ line (347.9 eV) that can be attributed to calcium compounds such as oxide, carbonate, sulfate, and silicate. It is suggested that calcium, being initially bonded to alginate carboxylate, was displaced by La(III) ions during biosorption.

5. Conclusions

SEM micrographs showed that the *Sargassum* sp. biomass surface is broadly colonized by diatoms. The assignments observed on EDX spectra are in agreement with the chemical composition expected for *Sargassum* sp. and diatoms.

La(III) biosorption hardly affects FTIR spectra. Systematic shifts of the bands were not observed in the FTIR spectra, but the contribution of carboxylate groups (mainly in alginate) on La(III) coordination was demonstrated with the overlap of amine/amide band by carboxylate antisymmetric stretching to form lanthanum bidentate complexes.

XPS spectra depicted the complexity of compounds on biosorbent surface, showing a large number of elements present in different bonding environments. The uptake reached up to 0.6 at.% for La(III) biosorption at 3.60 mmol L^{-1}. High-resolution O 1s spectra revealed the appearance of a new component after La(III) biosorption, which was associated to the interactions between La(III) ions and oxygenated compounds on the biomass. The La $3d_{5/2}$ spectra confirmed that three kinds of sites can be involved in La(III) biosorption: (a) oxygen atoms of alcohol and ether groups of polysaccharides (essentially from the alginate); (b) other oxygen atoms of alginate carboxylate groups; and (c) fucoidan sulfate ester groups. Furthermore, the spectral analysis indicates that diatom biosilica did not appear to contribute to La(III) biosorption. The decrease of calcium atomic fraction with the increase of the initial concentration of La(III) confirmed that metal biosorption occurs through an ion-exchange mechanism between Ca(II) and La(III).

Acknowledgments

R.C.O., P.H., and O.G.J. are thankful to Fundação de Amparo à Pesquisa do Estado de São Paulo (FAPESP) for the technical support. R.C.O, E.G., J.M.T., and O.G.J. thank to European Commission for the financial support for the Project BIOPROAM (Bioprocesos: Tecnologías limpias para la protección y sustentabilidad del medio ambiente) of the ALFA Research Program (AML/190901/06/18414/II-0548-FC-FA). R.C.O. and O.G.J. also thank to Coordenação de Aperfeiçoamento de Pessoal de Nível Superior (CAPES) and the Conselho Nacional de Desenvolvimento Científico e Tecnológico (CNPq) for the financial support in Brazil. The authors declare no competing financial interest.

Appendices. Supplementary material

Supplementary data associated with this article can be found, in the online version, at http://dx.doi.org/10.1016/j.cej.2013.11.042.

References

[1] F. Vegliò, F. Beolchini, Removal of metal by biosorption: a review, Hydrometallurgy 44 (1997) 301–316.
[2] B. Volesky, Biosorption: application aspects – process simulation tools, Process Metal. 11B (2001) 69–80.
[3] S.S. Ahluwalia, D. Goyal, Microbial and plant derived biomass for removal of heavy metals from wastewater, Bioresour. Technol. 98 (2007) 2243–2257.
[4] S. Deng, R. Bai, Removal of trivalent and hexavalent chromium with aminated polyacrylonitrile fibers: performance and mechanisms, Water Res. 38 (2004) 2424–2432.
[5] F. Vegliò, A. Esposito, A.P. Reverberi, Copper adsorption on calcium alginate beads: equilibrium pH-related models, Hydrometallurgy 69 (2002) 43–57.
[6] A.I. Zouboulis, M.X. Loukidou, K.A. Matis, Biosorption of toxic metals from aqueous solutions by bacterial strain isolated from metal-polluted soils, Process Biochem. 39 (2004) 909–916.
[7] Z. Aksu, Equilibrium kinetic modeling of cadmium (II) biosorption by *C. vulgaris* in a batch system: effect of temperature, Sep. Pur. Technol. 21 (2001) 285–294.
[8] M.M. Figueira, B. Volesky, H.J. Mathieu, Instrumental analysis of iron species biosorption by *Sargassum* biomass, J. Environ. Sci. Technol. 33 (1999) 1840–1846.
[9] G.M. Gadd, Biosorption: critical review of scientific rationale, environmental importance and significance for pollution treatment, J. Chem. Technol. Biotechnol. 84 (2008) 13–28.
[10] N. Li, R. Bai, Copper adsorption on chitosan–cellulose hydrogel beads: behaviors and mechanisms, Sep. Pur. Technol. 42 (2005) 237–247.
[11] W. Murphy, H. Hughes, P. McLoughlin, Cu(II) binding by dried biomass of red, green and brown macroalgae, Water Res. 41 (2007) 731–740.
[12] R.C. Oliveira, O. Garcia Jr., Study of biosorption of rare earth metals (La, Nd, Eu, Gd) by *Sargassum* sp. biomass in batch systems: physicochemical evaluation of kinetics and adsorption models, Adv. Mater. Res. 71–73 (2009) 605–608.
[13] R.C. Oliveira, M.C. Palmieri, O. Garcia Jr., Biosorption of metals: state of the art, general features, and potential applications for environmental and technological processes, in: S.S. Shaukat (Ed.), Progress in Biomass and Bioenergy Production, InTech, Rijeka, 2011, pp. 151–176.
[14] P.X. Sheng, Y.P. Ting, J.P. Chen, L.J. Hong, Sorption of lead, copper, cadmium, zinc, and nickel by marine algal biomass: characterization of biosorptive capacity and investigation of mechanisms, Colloid Interf. Sci. 275 (2004) 131–141.
[15] J. Yu, M. Tong, S. Sun, B. Li, Cystine-modified biomass for Cd(II) and Pb(II) biosorption, J. Hazard. Mater. 143 (2007) 277–284.
[16] D.L. Vullo, H.M. Ceretti, M.A. Daniel, S.A.M. Ramírez, A. Zalts, Cadmium, zinc and copper biosorption mediated by *Pseudonomas veronii* 2E, Bioresour. Technol. 99 (2008) 5574–5581.
[17] B. Godlewska-Zylkiewicz, Microorganisms in inorganic chemical analysis, Anal. Bioanal. Chem. 384 (2006) 114–123.
[18] M.C. Palmieri, O. Garcia Jr., P. Melnikov, Neodymium biosorption from acidic solutions in batch system, Process Biochem. 36 (2000) 441–444.
[19] J.M. Modak, K.A. Natarajan, Biosorption of metals using nonliving biomass: a review, in: Minerals Metallurgical Processing, Society For Mining Metallurgy and Exploration, vol. 12, Englewood, 1995, pp. 189–196.
[20] M.C. Palmieri, B. Volesky, O. Garcia Jr., Biosorption of lanthanum using *Sargassum fluitans* in batch system, Hydrometallurgy 67 (2002) 31–36.
[21] D. Kratochvil, B. Volesky, Advances in the biosorption of heavy metals, Tibtech 16 (1998) 291–300.
[22] K. Nadaffi, R. Nabizadeh, R. Saeedi, A.H. Mahvi, F. Vaezi, K. Yahgmaeian, A. Ghasri, S. Nazmara, Biosorption of lead(II) and cadmium(II) by protonated *Sargassum glaucescens* biomass in a continuous packed bed column, J. Hazard. Mater. 147 (2007) 785–791.
[23] B. Volesky, G. Naja, Biosorption: application strategies, in: S.T.L. Harrison, D.E. Rawlings, J. Petersen (Eds.), Proceedings of the 16th International Biotechnology Symposium, IBS – Compress Co., Cape Town, 2005, pp. 531–542.
[24] Y. Andrès, G. Thouand, M. Boualam, M. Mergeay, Factors influencing the biosorption of gadolinium by microorganisms and its mobilization from sand, Appl. Microbiol. Biotechnol. 54 (2000) 262–267.
[25] Y. Andrès, C. Gérente, Removal of rare earth elements and precious metal species by biosorption, in: P. Kotrba, M. Mackova, T. Macek (Eds.), Microbial Biosorption of Metals, Springer, Amsterdam, 2011, pp. 179–196.
[26] M. Arica, G. Bayramoglu, M. Yilmaz, M. Bektas, O. Genç, Biosorption of Hg^{2+}, Cd^{2+}, and Zn^{2+} by Ca-alginate and immobilized wood-rotting fungus *Funalia trogii*, J. Hazard. Mater. 109 (2004) 191–199.
[27] L. Philip, L. Iyengar, C. Venkobachar, Biosorption of U, La, Pr, Nd, Eu and Dy by *Pseudomonas aeruginosa*, J. Ind. Microbiol. Biotechnol. 25 (2000) 1–7.
[28] M. González-Dávila, J.M. Santana-Casiano, L.M. Laglera, Copper adsorption in diatom cultures, Mar. Chem. 70 (2000) 161–170.
[29] E.A. da Silva, E.S. Cossich, C.R. Granhen Tavares, L. Cardozo Filho, R. Guirardello, Modeling of copper(II) biosorption by marine alga *Sargassum* sp. in fixed-bed column, Process Biochem. 38 (2002) 791–799.
[30] V. Diniz, B. Volesky, Biosorption of La, Eu and Yb using *Sargassum* biomass, Water Res. 39 (2005) 239–247.
[31] V. Diniz, B. Volesky, Desorption of lanthanum, europium and ytterbium from *Sargassum*, Sep. Pur. Technol. 50 (2006) 71–76.
[32] V. Diniz, M.E. Weber, B. Volesky, G. Naja, Column biosorption of lanthanum and europium by *Sargassum*, Water Res. 42 (2008) 363–371.
[33] R.C. Oliveira, C. Jouannin, E. Guibal, O. Garcia Jr., Samarium(III) and praseodymium(III) biosorption on *Sargassum* sp.: batch study, Process Biochem. 46 (2011) 736–744.
[34] R.C. Oliveira, E. Guibal, O. Garcia Jr., Biosorption and desorption of lanthanum(III) and neodymium(III) in fixed-bed columns with *Sargassum* sp.: perspectives for separation of rare earth metals, Biotechnol. Prog. 28 (2012) 715–722.
[35] E. Valdman, L. Erijman, F.L.P. Pessoa, S.G.F. Leite, Continuous biosorption of copper and zinc by immobilized waste biomass of *Sargassum* sp., Process Biochem. 36 (2001) 869–873.
[36] M.G.A. Vieira, R.M. Oisiovici, M.L. Gimenes, M.G.C. Silva, Biosorption of chromium(VI) using a *Sargassum* sp. packed-bed column, Bioresour. Technol. 99 (2008) 3094–3099.

[37] K. Vijayaraghavan, D. Prabu, Potential of *Sargassum wightii* biomass for copper(II) removal from aqueous solutions: application of different mathematical models to batch and continuous biosorption data, J. Hazard. Mater. B 137 (2006) 558–564.

[38] K. Vijayaraghavan, M. Sathishkumar, R. Balasubramanian, Biosorption of lanthanum, cerium, europium, and ytterbium by a brown marine alga, *Turbinaria Conoides*, Ind. Eng. Chem. Res. 49 (2010) 4405–4411.

[39] G. Crini, Recent developments in polysaccharide-based materials used as adsorbents in wastewater treatment, Prog. Polym. Sci. 30 (2005) 38–70.

[40] L. Dambies, C. Guimon, S. Yiacoumi, E. Guibal, Characterization of metal ion interactions with chitosan by X-ray photoelectron spectroscopy, Colloids Surf. A: Physicochem. Eng. Aspects 177 (2001) 203–214.

[41] E. Guibal, Interactions of metal ions with chitosan-based sorbents: a review, Sep. Pur. Technol. 38 (2004) 43–74.

[42] H. Mimura, H. Ohta, K. Akiba, Y. Onodera, Uptake and recovery of ruthenium by alginate gel polymers, J. Nucl. Sci. Technol. 39 (2002) 655–660.

[43] V.C.G. Dos Santos, J.V.T.M. De Souza, C.R.T. Tarley, J. Caetano, D.C. Dragunsky, Copper ions adsorption from aqueous medium using the biosorbent sugarcane bagasse in natura and chemically modified, Water Air Soil Pollut. 216 (2011) 351–359.

[44] W. Xuejiang, C. Ling, X. Siqing, Z. Jianfu, J.-C. Chovelon, N.J. Renault, Biosorption of Cu(II) and Pb(II) from aqueous solutions by dried activated sludge, Miner. Eng. 19 (2006) 968–971.

[45] J.B. Hedrick, The global rare-earth cycle, J. Alloys Compd. 225 (1995) 609–618.

[46] T.S. Martins, P.C. Isolani, Terras-raras: aplicações industriais e biológicas, Quím. Nova 28 (2005) 111–117.

[47] T.P. Rao, R. Kala, On-line and off-line preconcentration of trace and ultratrace amounts of lanthanides, Talanta 63 (2004) 949–959.

[48] L.E. Graham, J.M. Graham, L.W. Wilcox, Algae, second ed., Benjamin Cummings, San Francisco, 2009.

[49] T.A. Davis, B. Volesky, A. Mucci, A review of the biochemistry of heavy metal biosorption by brown algae, Water Res. 37 (2003) 4311–4330.

[50] K.I. Draget, O. Smidsrod, G. Skjak-Braek, Alginates from algae, in: A. Steinbüchel, S.K. Rhee (Eds.), Polysaccharides and Polyamides in the Food Industry. Properties, Production, and Patents, Wiley-VCH, Weinheim, 2005, pp. 1–29.

[51] A.D. Holtkamp, Isolation, characterization, modification and application of fucoidan from *Fucus vesiculosus*, Ph.D. Thesis, Technischen Universität Carolo Wilhelmina, Braunschweig, 2009.

[52] C.M. DeRamos, A.E. Irwin, J.L. Nauss, B.E. Stout, ^{13}C NMR and molecular modeling studies of alginic acid binding with alkaline earth and lanthanide metal ions, Inorg. Chim. Acta 256 (1997) 69–75.

[53] N. Nestle, R. Kimmich, Heavy metal uptake of alginate gels studied by NMR microscopy, Colloids Surf. A: Physicochem. Eng. Aspects 115 (1996) 141–147.

[54] A. Gélabert, O.S. Pokrovsky, J. Schott, A. Boudou, A. Feurtet-Mazel, J. Mielczarski, E. Mielczarski, N. Mesmer-Dudons, O. Spalla, Study of diatoms/aqueous solution interface. I. Acid–base equilibria and spectroscopic observation of freshwater and marine species, Geochim. Cosmochim. Acta 68 (2004) 4039–4058.

[55] A.J. Milligan, F.M.M. Morel, A proton buffering role of silica in diatoms, Science 297 (2002) 1848–1850.

[56] G.R. Choppin, E.N. Rizkalla, Solution chemistry of actinides and lanthanides, in: K.A. Gschneider Jr., L. Eyring, G.R. Choppin, G.H. Lander (Eds.), Handbook on the Physics and Chemistry of Rare Earths, vol. 18, Elsevier Science B.V., Amsterdam, 1994, pp. 559–590.

[57] P. Thakur, P.N. Pathak, T. Gedris, G.R. Choppin, Complexation of Eu(III), Am(III) and Cm(III) with dicarboxylates: thermodynamics and structural aspects of the binary and ternary complexes, J. Solut. Chem. 38 (2009) 265–287.

[58] L. Fuks, D. Filipiuk, W. Lewandowski, Lanthanide ions complexation by uronic acids, J. Mol. Struct. 563–564 (2001) 587–593.

[59] N.B. Colthup, L.H. Daly, S.E. Wiberley, Introduction to Infrared and Raman Spectroscopy, third ed., Academic Press, San Diego, 1990.

[60] R.M. Silverstein, F.X. Webster, D. Kiemle, Spectrometric Identification of Organic Compounds, seventh ed., Wiley, Hoboken, 2005.

[61] N.P. Chandía, B. Matsuhiro, A.E. Vásquez, Alginic acids in *Lessonia trabeculata*: characterization by formic acid and FT-IR spectroscopy, Carbohydr. Polym. 46 (2001) 81–87.

[62] L. Pereira, A. Sousa, H. Coelho, A.M. Amado, P.J.A. Ribeiro-Claro, Use of FTIR, FT-Raman and ^{13}C-NMR spectroscopy for identification of some seaweed phycocolloids, Biomol. Eng. 20 (2003) 223–228.

[63] A. Pielesz, W. Biniaś, Cellulose acetate membrane electrophoresis and FTIR spectroscopy as methods of identifying a fucoidan in *Fucus vesiculosus* Linnaeus, Carbohydr. Res. 345 (2010) 2676–2682.

[64] S.K. Tam, J. Dusseault, S. Polizu, M. Ménard, J.-P. Hallé, L'H. Yahia, Impact of residual contamination on the biofunctional properties of purified alginates used for cell encapsulation, Biomaterials 27 (2006) 1296–1305.

[65] Y. Su, L. Yang, Z. Wang, C. Yan, S. Weng, J. Wu, Sugar complexes with neodymium nitrate. Spectroscopic and structural studies of two $Nd(NO_3)_3$-galactitol complexes, Carbohydr. Res. 338 (2003) 2029–2034.

[66] A. Synytsya, M. Urbanová, V. Setnička, M. Tkadlecová, J. Havlíček, I. Raich, P. Matjka, A. Synytsya, J. Čopíková, K. Volk, The complexation of metal cations by ^{d}-galacturonic acid: a spectroscopic study, Carbohydr. Res. 339 (2004) 2391–2405.

[67] L. Yang, Z. Wang, Y. Zhao, W. Tian, Y. Xu, S. Weng, J. Wu, Complexation of trivalent lanthanide cations by inositols in the solid state: crystal structure and an FT-IR study of $PrCl_3$·*myo*-inositol·$9H_2O$, Carbohydr. Res. 329 (2000) 847–853.

[68] L. Yang, D. Xie, Y. Xu, Y. Wang, S. Zhang, S. Weng, K. Zhao, J. Wu, Interactions between metal ions and carbohydrates. The coordination behavior of neutral erythritol to neodymium ion, J. Inorg. Biochem. 99 (2005) 1090–1097.

[69] S.K. Tam, J. Dusseault, S. Polizu, M. Ménard, J.-P. Hallé, L'H. Yahia, Physicochemical model of alginate-poly-L-lysine microcapsules defined at the micrometric/nanometric scale using ATR-FTIR, XPS, and ToF-SIMS, Biomaterials 26 (2005) 6950–6961.

[70] C.G. van Hoogmoed, H.J. Busscher, P. de Vos, Fourier transform infrared spectroscopy studies of alginate-PLL capsules with varying compositions, Mater. Res. A 67A (2003) 172–178.

[71] B. Tesson, C. Gaillard, V. Martin-Jézéquel, Brucite formation mediated by the diatom *Phaeodactylum tricornutum*, Mar. Chem. 109 (2008) 60–76.

[72] G.B. Deacon, R.J. Phillips, Relationships between the carbon-oxygen stretching frequencies of carboxylato complexes and the type of carboxylate coordination, Coord. Chem. Rev. 33 (1980) 227–250.

[73] R. Jarimavičiūtė-Žvalionienė, S. Tamulevičius, M. Andrulevičius, G. Statkutė, R. Tomašiūnas, V.J. Grigaliūnas, Effects of selenium treatment on composition and photoluminescence properties of porous silicon, J. Lumin. 127 (2007) 431–434.

[74] G. Lawrie, I. Keen, B. Drew, A. Chandler-Temple, L. Rintoul, P. Fredericks, L. Grøndhal, Interactions between alginate and chitosan biobolymers characterized using FTIR and XPS, Biomacromolecules 8 (2007) 2533–2541.

[75] S.-F. Lim, Y.M. Zheng, S.-W. Zou, J.P. Chen, Characterization of copper adsorption onto an alginate encapsulated magnetic sorbent by a combine FT-IR, XPS, and mathematical modeling study, Environ. Sci. Technol. 42 (2002) 9413–9421.

[76] Y.A. Teterin, A.Y. Teterin, A.M. Lebedev, K.E. Ivanov, Secondary electronic processes and the structure of X-ray photoelectron spectra of lanthanides in oxygen-containing compounds, J. Electron Spectrosc. Relat. Phenom. 137–140 (2004) 607–612.

[77] Y. Uwamino, T. Ishizuka, H. Yamatera, X-ray photoelectron spectroscopy of rare-earth compounds, J. Electron Spectrosc. Relat. Phenom. 34 (1984) 67–78.

[78] H. Yamada, T. Shimizu, A. Kurokawa, K. Ishii, E. Suzuki, MOCVD of high-dieletric-constant lanthanum oxide thin films, J. Electrochem. Soc. 150 (2003) G429–G435.

[79] A.V. Naumkin, A. Kraut-Vass, S.W. Gaarenstroom, C.J. Powell, NIST X-ray Photoelectron Spectroscopy Database, 2012. <http://srdata.nist.gov/xps/>.

[80] H. Corlett, B. Jones, Epiphyte communities on *Thalassia testudinum* from Grand Cayman, British West Indies: their composition, structure, and contribution to lagoonal sediments, Sediment. Geol. 194 (2007) 245–262.

[81] C. Dupraz, R.P. Reid, O. Braissant, A.W. Decho, R.S. Norman, P.T. Visscher, Processes of carbonate precipitation in modern microbial mats, Earth-Sci. Rev. 96 (2009) 141–162.

[82] R.C. Oliveira, Biossorção de terras-raras por *Sargassum* sp.: estudos preliminares sobre as interações metal–biomassa e a potencial aplicação do processo para a concentração, recuperação e separação de metais de alto valor agregado em colunas empacotadas, Ph.D. Thesis, Universidade Estadual Paulista, Araraquara, 2011.